On the Euler rotation angle and axis of a subgrid-scale stress model

By M. Saeedi†, B.-C. Wang† AND S. T. Bose

In this research, geometrical characteristics of the constitutive relation between the subgrid-scale (SGS) stress and filtered strain rate tensors are investigated based on the concept of Euler rotation angle and axis. Four different SGS stress models are studied using a priori tests by processing a comprehensive direct numerical simulation (DNS) data set of a zero-pressure-gradient transitional boundary-layer flow. The proposed approach is proven to be effective for demonstrating geometrical properties of a SGS stress model and for quantifying its degree of nonlinearity.

1. Introduction

Geometrical characterization of the frame fixed to a rigid body with respect to a reference frame has important applications in attitude dynamics (i.e., rotation dynamics between the frames), astrophysics, robotics and satellite control. By considering different fluid tensors required for accurate understanding of turbulent flows, similar approach can be applied to analysis of the tensorial geometrical relation between two tensors. Here, eigenframe refers to the orthonormal triad formed by three normalized eigenvectors of a real, symmetrical, second-order tensor.

In LES of turbulent flows, the constitutive relation between the subgrid-scale (SGS) stress tensor τ_{ij} and the filtered strain rate tensor $\bar{S}_{ij}$ is fundamentally important for SGS stress modelling. Betchov (1956) pioneered the application of Euler angle to the study of geometrical properties of the velocity gradient tensor. His method was later extended by Saffman & Pullin (1994), Pullin & Saffman (1994) and Misra & Pullin (1997) to study the eigenframe attitude of the velocity gradient, Reynolds stress, and SGS stress tensors. Horiuti (2003) and Tao *et al.* (2002) investigated the eigenframe of $-\tau_{ij}$ relative to that of $\bar{S}_{ij}$ using the axis-azimuth representation (which includes three angles: colatitude θ, longitude ϕ and azimuthal angle ζ). However, parametrization of the attitude of the eigenframe of $-\tau_{ij}$ and with respect to that of $\bar{S}_{ij}$ using the axis-azimuth representation is not uniquely defined, which depends upon the specific method that is adopted for decomposing the relative rotational motion between the two eigenframes. In view of this, Wang *et al.* (2006) suggested that use of Euler rotation angle and axis can uniquely describe the attitude of the eigenframe of $-\tau_{ij}$ relative to that of $\bar{S}_{ij}$. The method proposed by Wang *et al.* (2006) stems from the classical Euler's theorem, which utilizes only one special angle (i.e., Euler rotation angle χ) to quantify the relative rotation between two frames and only one special vector (i.e., Euler axis $\mathbf{q}$) to define the central axis of the rotation. Both the Euler rotation angle χ and Euler axis $\mathbf{q}$ are the natural invariants of the rotation matrix $\mathbf{R}$ (consisting of direction cosines). This provides an elegant method for unique parameterization of the relative rotation between the eigenframes of $-\tau_{ij}$ and $\bar{S}_{ij}$, which is not only intuitive for demonstrating

† Dept. of Mechanical Engineering, Univ. of Manitoba, Winnipeg, MB, R3T 5V6, Canada

the difference between SGS stress models in terms of their degrees of nonlinearity, but also effective in revealing nonlinear physics characteristic of a SGS stress tensor (such as the phenomenon of backscatter of kinetic energy between the subgrid and filtered scales).

In this research, the Euler rotation angle χ and Euler axis $\mathbf{q}$ proposed by Wang *et al.* (2006) will be further applied to the investigation of the constitutive relations of four different SGS stress models using an a priori approach. The a priori analysis will be conducted using a new comprehensive DNS data set of Wu & Moin (2013) for a zero-pressure-gradient transitional boundary-layer flow over a flat plate, and the concepts and values of the Euler rotation angle χ and Euler axis $\mathbf{q}$ will be rigorously examined against DNS data. This paper is organized as follows: in Section 2, the definition and mathematical properties of the Euler rotation angle χ and Euler axis $\mathbf{q}$ will be introduced; in Section 3, the a priori LES approach, DNS data set of Wu & Moin (2013) and four SGS stress models used in this research will be briefly described; in Section 4, a priori results on the Euler rotation angle and axis predicted by SGS models will be thoroughly analyzed and compared against the DNS data; and finally, in Section 5, the major conclusions of this research will be summarized.

2. Euler rotation angle and axis

Because both $-\tau_{ij}$ and $\bar{S}_{ij}$ are real symmetrical second-order tensors, they have three real eigenvalues that can be arranged in a descending order $\alpha \geq \beta \geq \gamma$. The three orthonormal eigenvectors corresponding to these three eigenvalues are represented by $\mathbf{e}_\alpha$, $\mathbf{e}_\beta$ and $\mathbf{e}_\gamma$, respectively, which together in this sequence can be used to form an orthonormal right-handed triad (eigenframe). According to Euler's Theorem (1776), every rotation between two rigid frames is equivalent to a rotation about a fixed axis (Euler axis) $\mathbf{q}$ through an angle (Euler rotation angle) χ. In this study, the Euler axis $\mathbf{q}$ is normalized, so that $|\mathbf{q}| = 1$. Figure 1 schematically shows the geometric relation between the eigenframes of $-\tau_{ij}$ and $\bar{S}_{ij}$. The relative rotation between the eigenframe of $-\tau_{ij}$ and that of $\bar{S}_{ij}$ vividly characterizes the degree of nonlinearity of a SGS stress tensor. Because the eigenframes of $-\tau_{ij}$ and $\bar{S}_{ij}$ are strictly aligned with each other in a linear SGS stress model, there is no relative rotation between them. Here, a linear SGS stress model refers to the modelling approach that satisfies $-\tau_{ij} \propto \bar{S}_{ij}$ (typical of the Boussinesq assumption). Furthermore, because the direction of an eigenvector is ambiguous (or, aliased), only the first quadrant of the eigenframe shown in Figure 1 is investigated.

In order to study the attitude dynamics between the eigenframe of $-\tau_{ij}$ and $\bar{S}_{ij}$, it is important to revisit the properties of the rotation matrix $\mathbf{R}$ between two orthonormal frames because $\mathbf{q}$ and χ are the so-called natural invariants of $\mathbf{R}$ (Angeles 1988). Assuming that $\mathcal{E} = [\mathbf{e}_1, \mathbf{e}_2, \mathbf{e}_3]$ and $\mathcal{E}' = [\mathbf{e}'_1, \mathbf{e}'_2, \mathbf{e}'_3]$ are the orthonormal absolute and relative (or, observer-referenced and object-referenced) frames, respectively, the rotation matrix can be determined using direction cosines of these two orthonormal frames,

$$R_{ij} = \mathbf{e}'_i \cdot \mathbf{e}_j = \cos(\mathbf{e}'_i, \mathbf{e}_j), \tag{2.1}$$

The rotation matrix has the following unique properties:

$$\mathbf{R}^T\mathbf{R} = \mathbf{R}\mathbf{R}^T = \mathbf{I}, \quad \mathbf{R}^{-1} = \mathbf{R}^T, \quad \det(\mathbf{R}) = \pm 1, \tag{2.2}$$

If $det(\mathbf{R}) = +1$, $\mathbf{R}$ is referred to as a proper rotation matrix, otherwise, it is called improper. A proper $\mathbf{R}$ reflects pure rotation whereas an improper $\mathbf{R}$ also involves reflection. In order to determine the two natural invariants of $\mathbf{R}$, the characteristics equation of its eigen system ($\mathbf{R}\mathbf{e} = \lambda\mathbf{e}$) needs to be considered,

$$\det(\mathbf{R} - \lambda\mathbf{I}) = -\lambda^3 + \mathrm{tr}(\mathbf{R})\lambda^2 - \mathrm{tr}(\mathbf{R})\lambda + 1 = 0, \tag{2.3}$$

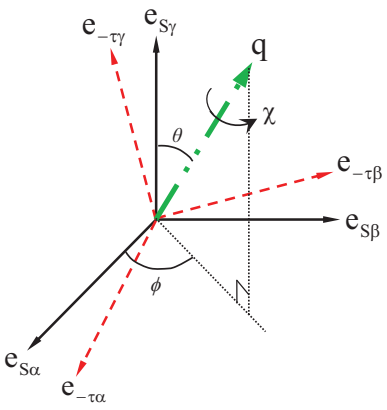

FIGURE 1. Euler rotation angle and axis between the eigenframes (right-handed) of $-\tau_{ij}$ and $\bar{S}_{ij}$.

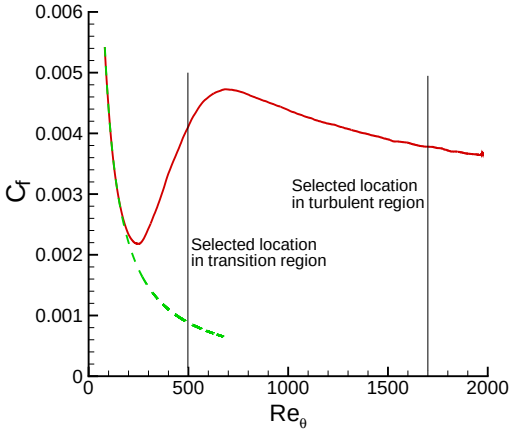

FIGURE 2. Averaged skin friction coefficient as a function of Re_θ. Dashed line: laminar theory, solid line: DNS (Wu & Moin 2013).

whose roots are the three eigenvalues of $\mathbf{R}$:

$$\lambda = +1, \quad e^{i\chi}, \quad e^{-i\chi}, \tag{2.4}$$

where $i \overset{\text{def}}{=} \sqrt{-1}$. The Euler equivalent axis $\mathbf{q}$ corresponds to the eigenvector of the real eigenvalue $\lambda = +1$. However, the Euler rotation angle χ is characterized by the phase of the other two eigenvalues. From Eq. (2.4), we obtain

$$\mathrm{tr}(\mathbf{R}) = \lambda_1 + \lambda_2 + \lambda_3 = 1 + 2\cos\chi, \tag{2.5}$$

which determines the Euler rotation angle as $\chi = \cos^{-1}\{[\mathrm{tr}(\mathbf{R}) - 1]/2\}$. The Euler axis $\mathbf{q} = [q_1, q_2, q_3]^T$ can be determined from the skew-symmetric part of $\mathbf{R}$ as

$$\mathbf{q}^\times = \frac{1}{2\sin\chi}(\mathbf{R}^T - \mathbf{R}), \tag{2.6}$$

where $\mathbf{q}^\times$ represents the following matrix:

$$\mathbf{q}^\times = \begin{bmatrix} 0 & -q_3 & q_2 \\ q_3 & 0 & -q_1 \\ -q_2 & q_1 & 0 \end{bmatrix}. \tag{2.7}$$

Conversely, the rotation matrix $\mathbf{R}$ can also be calculated using the Euler rotation angle and axis as

$$\mathbf{R} = \cos\chi\mathbf{I} + (1 - \cos\chi)\mathbf{q}\mathbf{q}^T - \sin\chi\mathbf{q}^\times. \tag{2.8}$$

From Eq. (2.5), the Euler rotational angle χ can be determined from the trace of $\mathbf{R}$, and from Eq. (2.6), the Euler rotation axis can be determined from Eq. (2.7) provided that $\mathrm{tr}(\mathbf{R}) \neq +3$ or -1. If $\mathrm{tr}(\mathbf{R}) = 3$ or -1, the system becomes singular and the axis of rotation cannot be directly determined from Eq. (2.6). In the case of $\mathrm{tr}(\mathbf{R}) = 3$, $\mathbf{R} = \mathbf{I}$, $\mathbf{q}$ is not defined and its direction is arbitrary. However, in the case that $\mathrm{tr}(\mathbf{R}) = -1$,

$$\mathbf{R} = 2\mathbf{q}\mathbf{q}^T - \mathbf{I}, \tag{2.9}$$

from which $\mathbf{q}$ can be determined.

3. Methodology

3.1. *A priori LES approach*

In order to conduct the current a priori study, the most recent comprehensive DNS data set for a zero-pressure-gradient transitional boundary-layer flow over a flat plate obtained by Wu & Moin (2013) is used. In total, $8192 \times 500 \times 256$ control volumes (in the streamwise, wall-normal and spanwise directions, respectively) were used in their DNS and the data set consists of 243 instantaneous snapshots of the flow field. The flow starts with a classical Blasius boundary layer profile with $Re_\theta = 80$, goes through transition (approximately between $Re_\theta = 250$ and 750), reaches fully turbulent state, and finally exits the domain at about $Re_\theta = 1850$. At the inlet of the domain, continuous free stream turbulence with 3% intensity was imposed. Different from their previous approaches (Wu & Moin 2009; Wu 2010), in order to trigger the transition, continuous free stream turbulence was generated using 25 independent temporally decaying blocks of homogeneous isotropic turbulence. Figure 2 shows the profile of the averaged skin friction coefficient as a function of Re_θ along the flat plate. In order to process the turbulent field using the a priori method, two specific streamwise locations in the transitional and turbulent regions are selected in our research, which correspond to $Re_\theta = 500$ and 1700, respectively.

The a priori procedure was performed following the method of Liu *et al.* (1994). The filtering operation at the grid and test-grid levels need to be explicitly specified. The discrete Gaussian filter proposed by Sagaut & Grohens (1999) was used to extract the SGS stress tensors. In our approach, the filter size ($\bar{\Delta}$) at the grid level was three times the local mesh size (Δ) for DNS in each direction (i.e., $\epsilon = \bar{\Delta}/\Delta = 3$), such that the control volume for LES is 27 times larger than that for DNS. In the dynamic modelling procedure, the filter size at the test-grid level ($\tilde{\bar{\Delta}}$) was twice the filter size at the grid level (i.e., $\tilde{\epsilon} = \tilde{\bar{\Delta}}/\bar{\Delta} = 2$). In this paper, the filtering process performed at the grid-level is denoted using an overbar and that at the test-grid level is denoted using a tilde. The SGS stress information can be extracted either directly by filtering the DNS data, or indirectly by using the SGS models. As a convention, the results on the Euler rotation angle and axis obtained using the first approach (without being influenced by SGS stress models) will be referred to as the DNS results in the remainder of this paper.

3.2. *SGS stress models*

The objective of this research is to investigate the tensorial geometrical property of the constitutive relations of four SGS stress models. The first model tested is the conventional dynamic Smagorinsky model (DM) (Germano *et al.* 1991; Lilly 1992), which expresses the SGS stress tensor as

$$\tau_{ij}^{*} \overset{\text{def}}{=} \tau_{ij} - \frac{\tau_{kk}}{3}\delta_{ij} = C_s \bar{\Delta}^2 |\bar{S}_{ij}| \bar{S}_{ij}, \tag{3.1}$$

where $\bar{S}_{ij} \overset{\text{def}}{=} (\partial \bar{u}_i/\partial x_j + \partial \bar{u}_j/\partial x_i)/2$ is the filtered strain rate tensor, $|\bar{S}_{ij}|$ is the norm of $\bar{S}_{ij}$, δ_{ij} is the Kronecker delta, and an asterisk superscript denotes the trace free form of a tensor. The dynamic model coefficient C_S can be obtained using the least squares method, viz.

$$C_S = -\frac{M_{ij}\mathcal{L}_{ij}}{M_{mn}M_{mn}}, \tag{3.2}$$

where $\mathcal{L}_{ij}$ is the resolved Leonard type stress defined as $\mathcal{L}_{ij} \overset{\text{def}}{=} \widetilde{\bar{u}_i\bar{u}_j} - \tilde{\bar{u}}_i\tilde{\bar{u}}_j$, and $M_{ij} \overset{\text{def}}{=} \alpha_{ij} - \tilde{\beta}_{ij}$ is a differential tensor. Here, $\alpha_{ij} \overset{\text{def}}{=} 2\tilde{\bar{\Delta}}^2|\tilde{\bar{S}}|\tilde{\bar{S}}_{ij}$ and $\beta_{ij} \overset{\text{def}}{=} 2\bar{\Delta}^2|\bar{S}|\bar{S}_{ij}$ are the test-grid and grid level base stress tensors, respectively.

The second model tested is the similarity model (SM) introduced by Liu *et al.* (1994), which calculates the SGS stresses as

$$\tau^*_{ij} = C_L\mathcal{L}_{ij}. \tag{3.3}$$

The model coefficient for the SM is set to $C_L = 0.45 \pm 0.15$.

The third model tested is the dynamic two parameter mixed model (DTPMM) of Morinishi & Vasilyev (2001), which is constructed using a combination of the scale similarity and Smagorinsky models,

$$\tau^*_{ij} = -2C_s\bar{\Delta}^2|\bar{S}_{ij}|\bar{S}_{ij} + C_L L^*_{ij}. \tag{3.4}$$

where

$$L_{ij} \overset{\text{def}}{=} \overline{\bar{u}_i\bar{u}_j} - \bar{\bar{u}}_i\bar{\bar{u}}_j. \tag{3.5}$$

The two coefficients can be determined using the least squares approach,

$$\begin{bmatrix} H^{z^*}_{ij}H^{z^*}_{ij} & -H^{z^*}_{ij}M_{ij} \\ -H^{z^*}_{ij}M_{ij} & M_{ij}M_{ij} \end{bmatrix} \cdot \begin{bmatrix} C_L \\ C_s \end{bmatrix} = \begin{bmatrix} \mathcal{L}^*_{ij}H^{z^*}_{ij} \\ \mathcal{L}^*_{ij}M_{ij} \end{bmatrix}, \tag{3.6}$$

where $H^z_{ij} = \widetilde{\bar{\bar{u}}_i\bar{\bar{u}}_i} - \tilde{\bar{\bar{u}}}_i\tilde{\bar{\bar{u}}}_j$.

The fourth model tested is the dynamic non-linear model (DNM) proposed by Wang & Bergstrom (2005). The DNM is based on an explicit nonlinear quadratic tensorial polynomial constitutive relation originally proposed by Speziale (1987) for modelling the Reynolds stress tensor in the Reynolds-averaged Navier-Stokes (RANS) approach. It employs three model coefficients dynamically calibrated using the local instantaneous velocity field. The DNM models the SGS stress tensor as

$$\tau^*_{ij} = -C_S\beta_{ij} - C_W\gamma_{ij} - C_N\eta_{ij}, \tag{3.7}$$

where the base tensors are defined as $\gamma_{ij} \overset{\text{def}}{=} 4\bar{\Delta}^2(\bar{S}_{ik}\bar{\Omega}_{kj} + \bar{S}_{jk}\bar{\Omega}_{ki})$ and $\eta_{ij} \overset{\text{def}}{=} 4\bar{\Delta}^2(\bar{S}_{ik}\bar{S}_{kj} - \bar{S}_{mn}\bar{S}_{nm}\delta_{ij}/3)$ (analogous to the definition of β_{ij}). Here, $\bar{\Omega}_{ij} \overset{\text{def}}{=} (\partial\bar{u}_i/\partial x_j - \partial\bar{u}_j/\partial x_i)/2$ is the filtered rotation rate tensor. Following the least squares procedure, the local dynamic model coefficients can be obtained,

$$\begin{bmatrix} M_{ij}M_{ij} & M_{ij}W_{ij} & M_{ij}N_{ij} \\ W_{ij}M_{ij} & W_{ij}W_{ij} & W_{ij}N_{ij} \\ N_{ij}M_{ij} & N_{ij}W_{ij} & N_{ij}N_{ij} \end{bmatrix} \cdot \begin{bmatrix} C_S \\ C_W \\ C_N \end{bmatrix} = \begin{bmatrix} L^*_{ij}M_{ij} \\ L^*_{ij}W_{ij} \\ L^*_{ij}N_{ij} \end{bmatrix}, \tag{3.8}$$

where $W_{ij} \overset{\text{def}}{=} \lambda_{ij} - \tilde{\gamma}_{ij}$ and $N_{ij} \overset{\text{def}}{=} \zeta_{ij} - \tilde{\eta}_{ij}$ are differential tensors, respectively (analogous to the definition of M_{ij}); and $\lambda_{ij} \overset{\text{def}}{=} 4\tilde{\bar{\Delta}}^2(\tilde{\bar{S}}_{ik}\tilde{\bar{\Omega}}_{kj} + \tilde{\bar{S}}_{jk}\tilde{\bar{\Omega}}_{ki})$ and $\zeta_{ij} \overset{\text{def}}{=} 4\tilde{\bar{\Delta}}^2(\tilde{\bar{S}}_{ik}\tilde{\bar{S}}_{kj} - \tilde{\bar{S}}_{mn}\tilde{\bar{S}}_{nm}\delta_{ij}/3)$ are base tensors at the test-grid level.

The constitutive relation of Eq. (3.7) includes three tensorial constituent components, i.e., β_{ij}, γ_{ij} and η_{ij}. The first term β_{ij} is the well-known Smagorinsky component that primarily relates to the SGS dissipation and forward scatter of turbulent kinetic energy (TKE) from the filtered to SGS motions; the second term, γ_{ij}, does not make any contribution to the TKE transfer between the filtered and subgrid scales, but it significantly improves the correlation between the exact τ_{ij} extracted from a DNS database and that predicted by the nonlinear model; and the third term η_{ij} contributes considerably to the

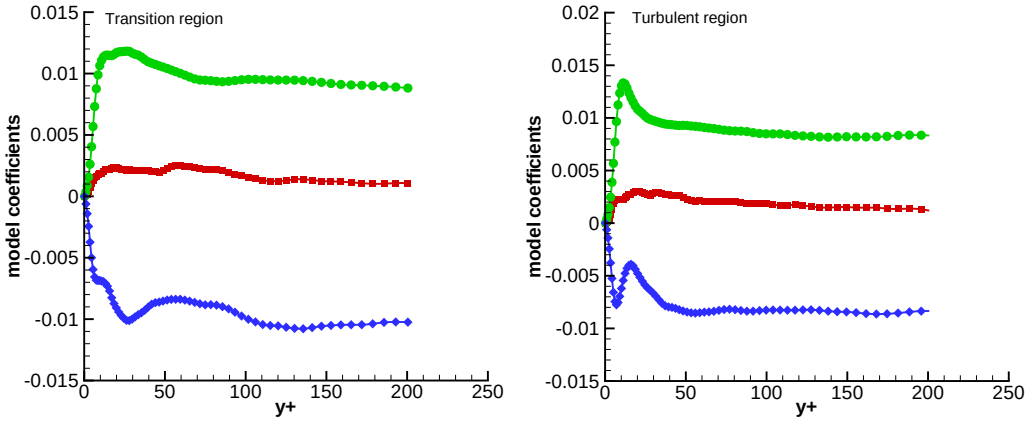

(a) $Re_\theta = 500$ (b) $Re_\theta = 1700$

FIGURE 3. Time and spanwise averaged profiles of the model coefficients for the DNM at two different streamwise locations. Squares: C_S, round dots: C_W, diamonds: C_N.

backscatter of TKE from the subgrid to the filtered scales (Wang & Bergstrom 2005). The three features mentioned above; namely, an adequate SGS dissipation level, a high correlation coefficient between the model and exact SGS stresses in a priori LES test, and a realistic representation of the TKE backscatter, are among the most important criteria for developing a high-fidelity SGS stress model. It has been observed that the DNM can be applied locally without any local averaging (or, clipping) techniques in calculation of its three coefficients in several test cases for low Reynolds number turbulent flows (Wang *et al.* 2006, 2008). Figures 3a and 3b show the time and spanwise averaged coefficients based on a priori LES processing of the DNS data. Calculation of the three local dynamic coefficients directly based on Eq.(3.8) has been stable during the current study, confirming the robustness of the DNM previously observed in a posteriori LES tests. The coefficient profiles clearly reflect the effects of wall anisotropy on SGS motions. Near the wall, all three coefficients approach zero indicating that the SGS stress tensor modelled by the DNM is automatically deactivated in the near-wall region where the viscous forces dominate.

4. Result analysis

Figures 4a and 4b show the time and spanwise averaged vertical profiles of the Euler rotation angle predicted by different SGS models in comparison with the DNS results. Although the predictions of χ by the SM, DTPMM and DNM are in general agreement with the DNS results, the DTPMM slightly outperforms the SM and DNM, especially in the central turbulent region of the boundary layer. The Euler rotation angle and Euler axis are very effective in demonstrating the degree of nonlinearity of a SGS stress model. For the DM of Lilly (1992), the eigenframe of $-\tau_{ij}$ is strictly aligned with that of $\bar{S}_{ij}$, which results in a unique singularity condition: $\mathbf{R} \equiv \mathbf{I}$, $\chi \equiv 0^\circ$ and the orientation of $\mathbf{q}$ being undefined.

In contrast to the linear DM, the constitutive relations for the SM, DTPMM and DNM all model $-\tau_{ij}$ as a nonlinear function of $\bar{S}_{ij}$. Consequently, rotation between the eigenframe of modelled $-\tau_{ij}$ and that of $\bar{S}_{ij}$ exists in a general case. Therefore, it is expected that the value of χ predicted by the SM, DTPMM and DNM all deviate from 0°

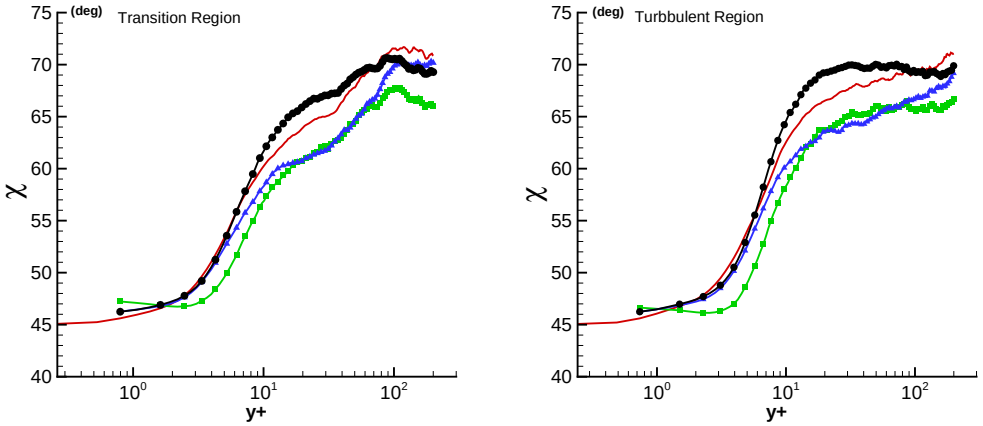

(a) $Re_\theta = 500$ (b) $Re_\theta = 1700$

FIGURE 4. Time and spanwise averaged Euler angle profile at two streamwise locations. Solid line: DNS, line with squares: DNM, line with triangles: DTPMM, line with round dots: SM.

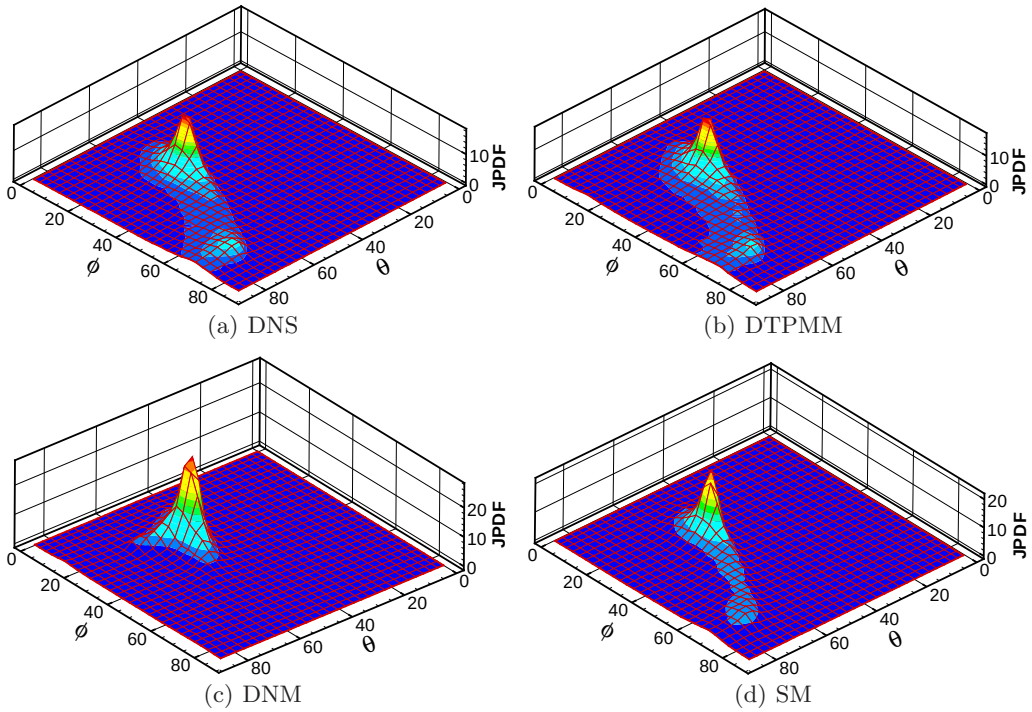

(a) DNS (b) DTPMM

(c) DNM (d) SM

FIGURE 5. Two-dimensional JPDF of colatitude θ and longitude ϕ for describing the orientation of the Euler axis within the viscous sublayer ($y^+ = 2.18$) of the transition region ($Re_\theta = 500$).

(a signature of linearity). Furthermore, from Eq. (2.6), if $\chi \neq 0°$, the Euler axis $\mathbf{q}$ exists. The physical feature that $\chi \neq 0°$ for the SM, DTPMM and DNM is evident in Figures 4a and 4b. It is interesting to observe that the Euler angles predicted by both DNS and LES methods converge to 45° as the wall is approached. The observation is consistent with the report of Wang *et al.* (2006). However, a rigorous analytical explanation for this special

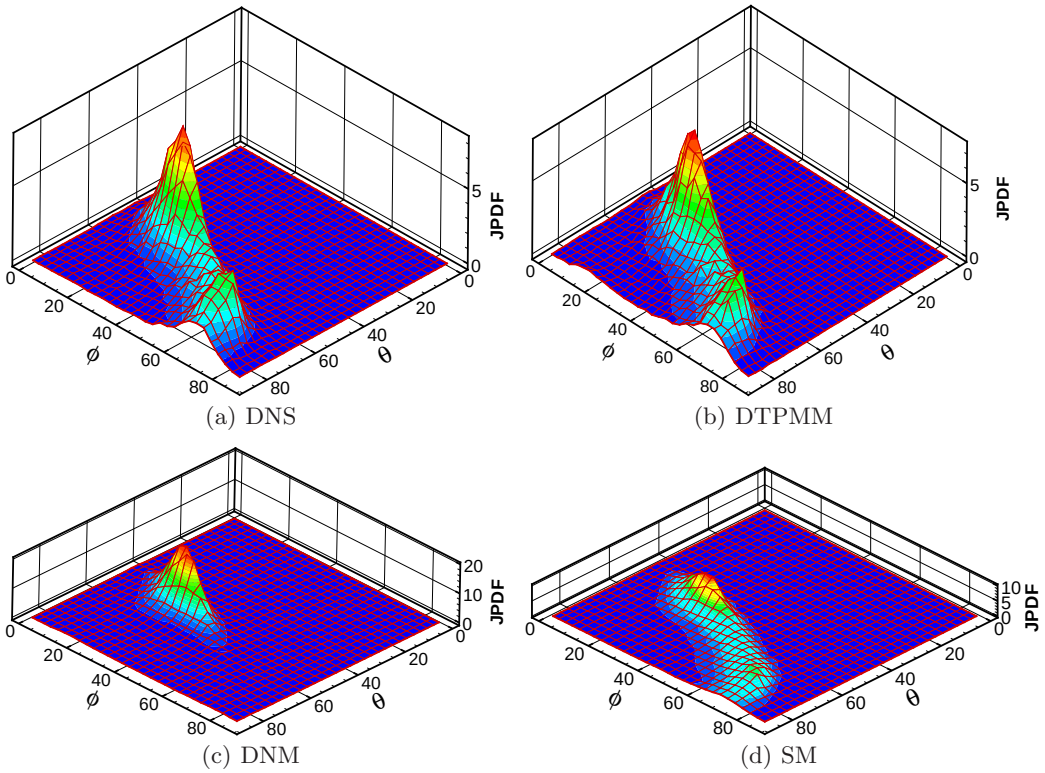

FIGURE 6. Two-dimensional JPDF of colatitude θ and longitude ϕ for describing the orientation of the Euler axis within the viscous sublayer ($y^+ = 2.02$) of the turbulent region ($Re_\theta = 1700$).

near-wall behavior is still lacking at this stage. As the distance from the wall increases, the value of χ keeps increasing until it reaches approximately 70° at the edge of the boundary layer. This indicates that the maximum rotation between the eigenframes of $-\tau_{ij}$ and $\bar{S}_{ij}$ (corresponding to the maximum degree of nonlinearity of SGS modelling) takes place where the wall effects are minimum and turbulent activities are at peak.

In order to visualize the orientation of Euler axis, two parameters: colatitude θ and longitude ϕ, can be used (see Figure 1). Assuming random orientation of the Euler axis in a three-dimensional Cartesian space, then the terminus of the unit vector $\mathbf{q}$ is uniformly distributed on the surface of a unit sphere with respect to the so-called solid angle (defined as $S_\Sigma = \iint_\Sigma \sin\theta d\theta d\phi \approx \sin\theta \cdot \Delta\theta \cdot \Delta\phi$, where Σ is the area of the bin for statistics on surface of the unit sphere). As demonstrated by Tao *et al.* (2002), it is appropriate to evaluate the two-dimensional joint PDF (JPDF) based on $\cos\theta$ and ϕ because it naturally includes the spherical effect through the solid angle, i.e., $S_\Sigma \approx \sin\theta \cdot \Delta\theta \cdot \Delta\phi = -\Delta(\cos\theta) \cdot \Delta\phi$.

As mentioned above, for the DM (Lilly 1992), the orientation of $\mathbf{q}$ is undefined corresponding to a special singularity condition unique to a linear SGS stress model. The statistics were calculated based on 30×30 bins, which give an uncertainty of $\pm 1.5°$. Figures 5a-d show JPDF(θ, ϕ) predicted by DNS and by a priori LES based on the DTPMM, DNM and SM within the viscous sublayer (at $y^+ = 2.18$) of the transitional region (for $Re_\theta = 500$). As evident in these Figures, the most probable mode for the

Euler axis orientation is about ($\theta = 50°$, $\phi = 25°$), which feature has been well predicted by the SM, DTPMM and DNM (in comparison with the DNS results). Figures 6a-d show JPDF(θ, ϕ) within the viscous sublayer (at $y^+ = 2.02$) of the turbulent region (for $Re_\theta = 1700$). In the DNS results shown in Figure 6a, there are two probable modes. The primary mode corresponds to approximately ($\theta = 50°$, $\phi = 10°$) and the secondary mode corresponds to approximately ($\theta = 70°$, $\phi = 60°$). The prediction of the primary mode by the SM is not as satisfactory as the DTPMM and DNM. However, the DNM fails to predict the secondary mode. In both Figures 5 and 6, the DTPMM outperforms slightly the SM and DNM in terms of the prediction of the orientation of the Euler axis.

However, it needs to be indicated that in both Figures 5 and 6, JPDFs are demonstrated only for the viscous sublayer. This is because the orientation of the Euler axis in the buffer and logarithmic regions is more toward random distribution (the JPDFs are not shown here due to the restriction on the length of the paper). The conclusions on comparison of SGS model performances based on Figures 5 and 6 should not be generalized. This is because SGS stress models are fully activated in a region where turbulent effects dominate and are the least active in the viscous sublayer where viscous forces dominate. In view of this, we conclude that although both Euler rotation angle and axis are natural invariants of rotation matrix $\mathbf{R}$, the Euler rotation angle is more useful and convenient for demonstrating intrinsic geometrical properties of the constitutive relation of a SGS stress model and can be viewed as a fingerprint of the model.

5. Conclusion

From the viewpoint of tensor geometry, the nonlinearity of a SGS stress model is caused by relative rotation of the eigenframe of $-\tau_{ij}$ with respect to that of $\bar{S}_{ij}$. In order to investigate this tensorial geometrical property of SGS stress models, a priori LES was performed based on post-processing of the new DNS data of Wu & Moin (2013) on a zero-pressure-gradient transitional boundary-layer flow. Two specific streamwise locations (corresponding to $Re_\theta = 500$ and 1700, respectively) were selected to study the flow physics in the transitional and turbulent regions.

It is confirmed in the current a priori tests that the proposed Euler rotation angle and Euler axis are very effective in demonstrating the degree of nonlinearity of a SGS stress model. For the DM of Lilly (1992), the eigenframe of $-\tau_{ij}$ is strictly aligned with that of $\bar{S}_{ij}$, which results in a unique singularity condition: $\mathbf{R} \equiv \mathbf{I}$, $\chi \equiv 0°$ and the orientation of $\mathbf{q}$ being undefined. In contrast, owing to the nonlinear effects, $\chi \neq 0°$ is expected for the SM, DTPMM and DNM in a general case. For the boundary-layer flow studied, the values of χ predicted by the SM, DTPMM and DNM all converge to 45° at the wall and increase to approximately 70° at the edge of the boundary layer. This indicates that the maximum rotation between the eigenframes of $-\tau_{ij}$ and $\bar{S}_{ij}$ takes place where the wall anisotropic effects are the minimum and turbulent motions are the most active. Although both Euler rotation angle and axis are natural invariants of rotation matrix $\mathbf{R}$, the Euler rotation angle is more useful and convenient for demonstrating intrinsic geometrical properties of the constitutive relation of a SGS stress model.

Acknowledgments

This work is supported jointly by the Natural Sciences and Engineering Research Council (NSERC) of Canada and Center for Turbulence Research (CTR) at Stanford University. Computing resources and DNS data sets are provided by CTR. The authors thank Pro-

fessors P. Moin and J. A. Domaradzki for their support and guidance, and the CTR Summer Program hosts and participants for the beneficial discussions.

REFERENCES

Angeles, J. 1988 *Rational Kinematics*. New York: Springer-Verlag.

Betchov, R. 1956 An inequality concerning the production of vorticity in isotropic turbulence. *J. Fluid Mech.* **1**, 497–504.

Germano, M., Piomelli, U., Moin, P. & Cabot, W. H. 1991 A dynamic subgrid scale eddy viscosity model. *Phys. Fluids A* **3**, 1760–1765.

Horiuti, K. 2003 Roles of non-aligned eigenvectors of strain-rate and subgrid-scale stress tensors in turbulence generation. *J. Fluid Mech.* **491**, 65–100.

Lilly, D. K. 1992 A proposed modification of the Germano subgrid-scale closure method. *Phys. Fluids A* **4**, 633–635.

Liu, S., Meneveau, C. & Katz, J. 1994 On the properties of similarity subgrid-scale models as deduced from measurements in a turbulent jet. *J. Fluid Mech.* **275**, 83–119.

Misra, A. & Pullin, D. I. 1997 A vortex-based subgrid stress model for large-eddy simulation. *Phys. Fluids* **9**, 2443–2454.

Morinishi, Y. & Vasilyev, O. V. 2001 A recommended modification to the dynamic two-parameter mixed subgrid scale model for large eddy simulation of wall bounded turbulent flow. *Phys. Fluids* **13**, 3400–3410.

Pullin, D. I. & Saffman, P. G. 1994 Reynolds stress and one dimensional spectra for a vortex model of homogeneous anisotropic turbulence. *Phys. Fluids* **6**, 1787–1796.

Saffman, P. G. & Pullin, D. I. 1994 Anisotropy of the Lundgren-Townsend model of fine-scale turbulence. *Phys. Fluids* **6**, 802–807.

Sagaut, P. & Grohens, R. 1999 Discrete filters for large eddy simulation. *Int. J. Numer. Meth. Fluids* **31**, 1195–1220.

Speziale, C. G. 1987 On nonlinear k–l and k–ϵ models of turbulence. *J. Fluid Mech.* **178**, 459–475.

Tao, B., Katz, J. & Meneveau, C. 2002 Statistical geometry of subgrid-scale stresses determined from holographic particle image velocimetry measurements. *J. Fluid Mech.* **457**, 35–78.

Wang, B.-C. & Bergstrom, D. 2005 A dynamic nonlinear subgrid-scale stress model. *Phys. Fluids* **17**, 035109.

Wang, B.-C., Yee, E. & Bergstrom, D. 2006 Geometrical description of subgrid-scale stress tensor based on Euler axis/angle. *AIAA J.* **44**, 1106–1110.

Wang, B.-C., Yee, E., Bergstrom, D. & Iida, O. 2008 New dynamic subgrid-scale heat flux models for large-eddy simulation of thermal convection based on the general gradient diffusion hypothesis. *J. Fluid Mech.* **640**, 125–163.

Wu, X. 2010 Establishing the generality of three phenomena using a boundary layer with free-stream passing wakes. *J. Fluid Mech.* **664**, 193–219.

Wu, X. & Moin, P. 2009 Direct numerical simulation of turbulence in a nominally zero-pressure-gradient flat-plate boundary layer. *J. Fluid Mech.* **630**, 5–41.

Wu, X. & Moin, P. 2013 Visualization of flat-plate boundary layer with continuous freestream turbulence. In preparation.